

RESEARCH ARTICLE

Open Access



Improved homology modeling of the human & rat EP₄ prostanoid receptors

Melissa C. Holt, Chi S. Ho, M. Inés Morano, Stephen D. Barrett and Adam J. Stein*

Abstract

Background: The EP₄ prostanoid receptor is one of four GPCRs that mediate the diverse actions of prostaglandin E₂ (PGE₂). Novel selective EP₄ receptor agonists would assist to further elucidate receptor sub-type function and promote development of therapeutics for bone healing, heart failure, and other receptor associated conditions. The rat EP₄ (rEP₄) receptor has been used as a surrogate for the human EP₄ (hEP₄) receptor in multiple SAR studies. To better understand the validity of this traditional approach, homology models were generated by threading for both receptors using the RaptorX server. These models were fit to an implicit membrane using the PPM server and OPM database with refinement of intra and extracellular loops by Prime (Schrödinger). To understand the interaction between the receptors and known agonists, induced-fit docking experiments were performed using Glide and Prime (Schrödinger), with both endogenous agonists and receptor sub-type selective, small-molecule agonists. The docking scores and observed interactions were compared with radioligand displacement experiments and receptor (rat & human) activation assays monitoring cAMP.

Results: Rank-ordering of in silico compound docking scores aligned well with in vitro activity assay EC₅₀ and radioligand binding K_i. We observed variations between rat and human EP₄ binding pockets that have implications in future small-molecule receptor-modulator design and SAR, specifically a S103G mutation within the rEP₄ receptor. Additionally, these models helped identify key interactions between the EP₄ receptor and ligands including PGE₂ and several known sub-type selective agonists while serving as a marked improvement over the previously reported models.

Conclusions: This work has generated a set of novel homology models of the rEP₄ and hEP₄ receptors. The homology models provide an improvement upon the previously reported model, largely due to improved solvation. The hEP₄ docking scores correlates best with the cAMP activation data, where both data sets rank order Rivenprost>CAY10684 > PGE₁ ≈ PGE₂ > 11-deoxy-PGE₁ ≈ 11-dexoy-PGE₂ > 8-aza-11-deoxy-PGE₁. This rank-ordering matches closely with the rEP₄ receptor as well. Species-specific differences were noted for the weak agonists Sulprostone and Misoprostol, which appear to dock more readily within human receptor versus rat receptor.

Keywords: Prostaglandin E₂, Prostaglandin E₂ receptor, Prostaglandin E₂ receptor subtype 4, PGE₂, EP₄, Homology model, Structure-based drug design, Bone healing, Heart failure

Background

Prostaglandin E₂ (PGE₂) in humans is an ubiquitous arachidonic acid-cyclooxygenase (COX) cascade product that mediates a multitude of signaling roles through activation of the GPCR superfamily-member E-type prostanoid receptors 1–4 (EP_{1–4}) [1]. The roles of functionally related EP receptors have been widely

investigated, and the receptors have been considered as therapeutic targets for a variety of indications including cancer, asthma, inflammation, heart failure, colitis, ischemia, and osteoporosis [2–5]. Selective EP₄ modulators have been sought to provide the benefits of target modulation while limiting side effects arising from the modulation of the other receptor subtypes. EP₄ is coupled to G protein-dependent pathways through G_{as} and G_{ai}, modulating adenylate cyclase activity and synthesis of intracellular cAMP. In addition to signaling through cAMP, biased agonism has been shown to play a role in

* Correspondence: astein@caymanchem.com

This manuscript was initially submitted to BMC Structural Biology on 15 June 2018 and was peer reviewed at that journal
Cayman Chemical Co, 1180 E. Ellsworth Rd, Ann Arbor, MI 48108, USA



the EP₄ downstream signaling through the β -catenin and β -arrestin pathways [3, 6, 7].

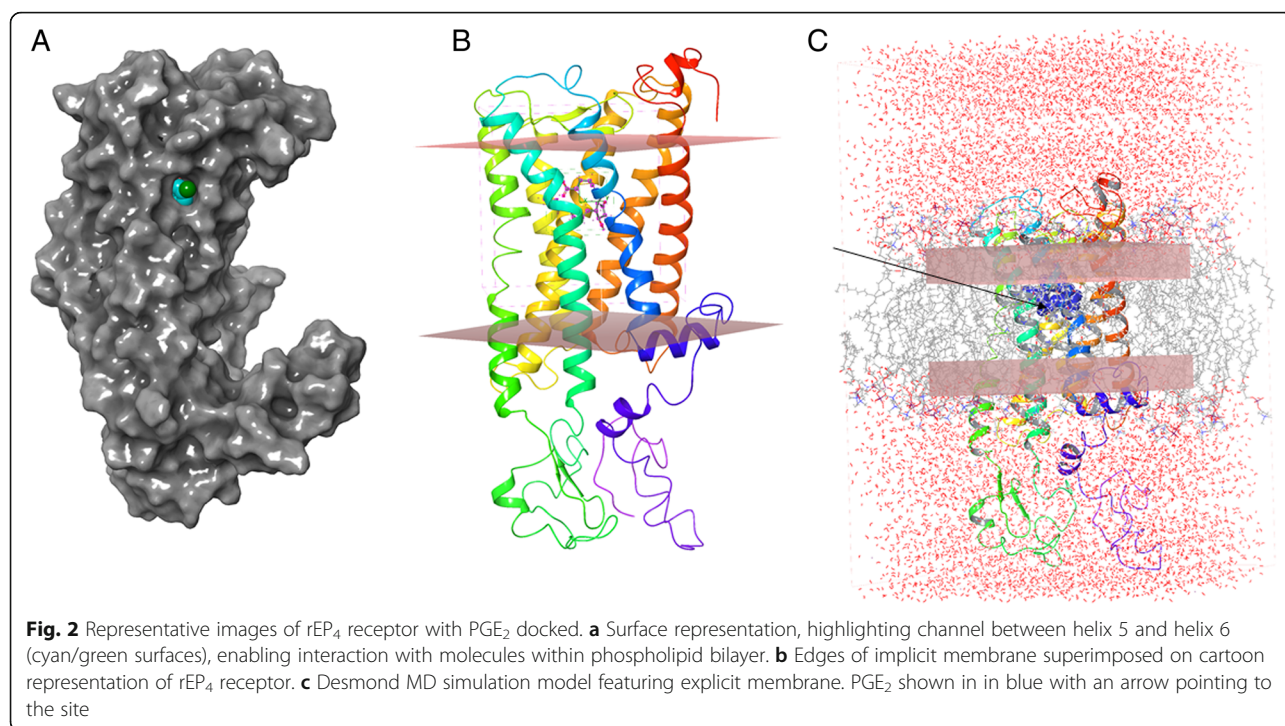
GlaxoSmithKline, Roche Holding AG, Ono Pharmaceuticals and Merck and Co. have targeted EP₄ with γ -lactam SAR programs [3, 8]. Multiple industrial drug-discovery programs have utilized the rat EP₄ (rEP₄) receptor as a surrogate for the human EP₄ (hEP₄) receptor in screening assays and animal models to identify lead compounds for development [9–15]. Potent, selective γ -lactam small molecule PGE₂ mimic EP₄ agonists were discovered using these screens and have advanced to various stages of preclinical and clinical development for several indications [9, 16]. Elimination of the stereocenter at the α -chain has been shown to be tolerated, beginning first with the discovery of 8-aza-11-deoxy-PGE₁ [17]. Highly selective, potent agonists such as Roche 31 (CAY10684) have been reported [16]. Likewise, the role of agonists such as Rivenprost (Ono-4819) within bone health has been well established [14]. Additionally, full and partial agonists of differing chemical classes have been identified, including GSK's reporting of non-prostanoid selective EP₄ agonists [18]. Within the classes of prostanoid agonists, species selectivity and potency differences have been noted, including Sulprostone and Misoprostol, where both show significantly increased potency for the human EP₄ receptor over rat receptor [19]. There is no reported mechanism driving the species difference between the rat and human receptors.

No known x-ray crystal structure of EP₄ exists from any species. Mutational studies of hEP₄ have implicated the hydroxyl of T168 as critical for PGE₂ binding [20]. While currently no experimental structural data for EP₄ exists, threading and docking studies have been performed with the hEP₄ receptor. That study implicates a set of polar contacts comprising a binding motif of Y186^(5.40), F191^(5.45), S103^(3.41), S285^(6.48), D311^(7.35) [21]. Since publication of these studies, threading methodologies have advanced where solvation models have been improved [22, 23]. With the aim of better understanding the binding event of PGE₂, evaluating the differences between the hEP₄ and rEP₄ receptors and to enable in silico drug discovery efforts, a homology modeling and docking study was undertaken focusing on these receptors. These models have been thoroughly validated by comparisons to binding and activation data.

Results

All reported models have been deposited to the ModelArchive (<https://www.modelarchive.org/>) [24, 25]. Sequence alignment and secondary structural prediction of the canonical 7 transmembrane helices are described in Fig. 1, as predicted using TCoffee Espresso Server

[26, 27]. Between helices 4 and 5, a set of anti-parallel β -sheets form the cap of the receptors. Amino acid sequence alignment of the full-length rEP₄ and hEP₄ shows that they are 88% identical. Structural alignment of hEP₄ and rEP₄ models have an RMSD of 0.42 Å, suggesting differences between the proteins are subtle. The global structure of the human and rat EP₄ homology models match well with the previously reported model (Fig. 2) [21]. A comparison of the hEP₄ receptor homology models generated by Swiss-model and RaptorX is shown in Table 1. The ERRAT2 quality score, which is a measure of the quality of non-bonded interactions in comparison to high resolution structures, suggests that the RaptorX model of hEP₄ was superior to the Swiss-model generated structure (Table 1) [28]. The model B-factor, a measure of uncertainty within the model, was larger within the RaptorX model. The Swiss-model featured loop deletions and truncations of the N-terminal and C-terminal regions of the receptor (regions of lower confidence) which improved the model B-factor. The Ramachandran plots from both models of hEP₄ were similar (Table 1 & Additional file 1: Figure S1). Bond angle deviations and bond length deviations in both models were low (Table 1). Z-score, a measure of acceptable bond lengths, phi (ϕ) and psi (ψ) angles, and flags of distortions within planes, was used to identify geometry outliers. Within the hEP₄ Swiss-model, Z-score outliers near the predicted binding site were identified including residues Y165 and Y188^(5.42) with scores of 19.66 and 19.10, respectively (Additional file 2: Figure S2). These geometric outliers near the reported binding site within the Swiss-model were of concern. Z-score outliers were identified within the hEP₄ RaptorX model, including H129 (5.88), Y130 (7.55), were less significant compared to the Swiss-model structure (Additional file 2: Figure S2). Outliers within the rEP₄ RaptorX model included F102 (11.49), H129 (8.22), H229-S234 (9.55, 10.09, 7.56, 7.56, 10.68, 5.02), A264 (10.49), and A265 (7.89) (data not shown). RaptorX model statistics are provided in full in (Additional file 9: Table S1). The model scores for the RaptorX hEP₄ and rEP₄ models were 269 and 268, respectively, where a score equaling sequence length is perfectly ideal (Additional file 9: Table S1). The uSeq percentages were nearly 60%, indicating a high confidence in the global structural fold (Additional file 9: Table S1). uGDT scores were > 100 for the RaptorX models with nGDT < 50, suggesting that specific regions of the model have increased uncertainty (SI Tale 1). The proposed binding sites are within the helical structure of the proteins, where the models provide the most confidence. An alignment of Squid Rhodopsin (PDB ID: 2ZIIY) and RaptorX hEP₄ model is shown in Fig. 3a with an alignment RMSD scoring function, displaying that the



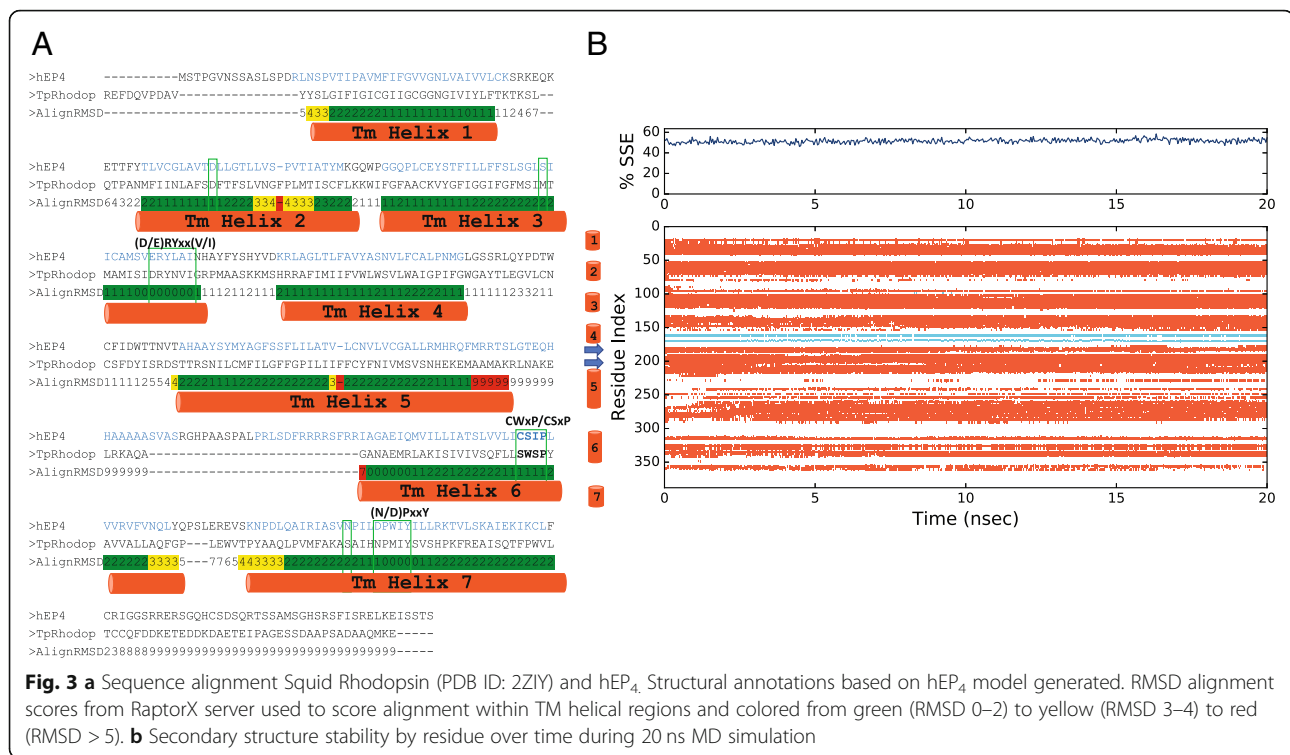
agonists displayed greater binding within the human receptor versus the rat [19]. The structures of each are described in Fig. 4. Docking and scoring experiments properly rank-ordered the known agonists by docking score relative to each other and predicted the species-specific binding differences, more so in the case of Sulprostone (Table 2). The human model implicated S103^(3.41) with an H-bond to the N-(methylsulfonyl) formamide tail on the α -chain of Sulprostone, an interaction which was replaced with Y188^(5.42) within the rat model with an increase in distance. This observation supports the role of hS103^(3.41) to rG103^(3.41) in species-specific selectivity. MM-GBSA scoring shows a nearly – 20 kcal/mol difference in binding of Misoprostol and Sulprostone between the human and rat receptors, matching with the predicted species selectivity. A structural overlay of the docked poses is shown in Fig. 5.

Table 1 Comparison of hEP₄ models where the RaptorX model shows a better score for non-bonded interactions

	Swiss-model	RaptorX
B Factor (\AA^2)	0.578	63.223
Bond Angle Dev. ($^\circ$)	2.118	2.242
Bond Length Dev. (\AA)	0.015	0.013
Steric Clashes	0	1
Ramachandran Favored (%)	91.25	90.25
Ramachandran Allowed (%)	6.88	5.75
ERRAT2 Quality	69.677	87.056

GSK recently reported an SAR series with binding data for several non-prostanoid EP₄ agonists [18]. The highest and lowest affinity compounds from this series corresponded to the non-prostanoid, fused benzoin-dol-1(3H)-one core with either a di-*p*-ethoxy substitution (CCL17464,2) or di-*p*-*n*-hexoxy substitution (CCL17464,19) (Fig. 4). These weak agonists were submitted for docking and scoring experiments and the model properly rank-ordered the pairing within the hEP₄ model which correlated well with reported binding affinities (Table 2). This suggested that the model could handle predictions using both prostanoid and non-prostanoid scaffolds. An overlay of the docked pose of CCL17464,2 versus the pose of PGE₂ is shown in Fig. 6.

Docking experiments were performed with a series of EP₄ agonists of biological interest towards better understanding the binding of prostanoid agonists and to continue to validate our model. The prostanoid derived agonists in Fig. 4 were submitted for an induced fit docking experiment in both hEP₄ and rEP₄. A plot of Glide scores versus Emodel scores from a representative experiment is shown in Additional file 5: Figure S5. Poses with larger absolute values for both metrics were favored and selected as top poses. The highest scoring pose of PGE₂ within hEP₄, featured a hydrogen bonding network between the 15-hydroxyl of PGE₂ in both the sidechain and backbone of S103^(3.41) (Fig. 7). S285^(6.48) sidechain serves as a hydrogen bond donor to the α -chain carboxylate (Fig. 7). The 11-hydroxyl of PGE₂ also forms a hydrogen bonding network between N321^(7.45) and



D65^(2.50) (Fig. 7). MD simulation shows a large amount of interactional flexibility within the binding event. D65^(2.50), S103^(3.41) serve as protein-ligand contact points throughout the entire simulation (Fig. 8). Polar contacts are exchanged through the simulation, D65^(2.50) makes contacts with 15-hydroxyl or 11-hydroxyl, N321^(7.45) makes contacts with 11-hydroxyl or 15-hydroxyl, S103^(3.41) makes contacts with carboxylate or 15-hydroxyl, and S285^(6.48) makes contacts with carboxylate or 15-hydroxyl. The α -chain carboxylate was observed to be highly flexible in its orientation, with a wide variety of torsions sampled. The radius of gyration, a measure of extendedness of a ligand and equivalent to its principal moment of inertia, hovered between 4.25 Å and 4.5 Å points to a stable orientation of the agonist within the binding pocket throughout the simulation (data not shown).

The residue specific interactions between PGE₂ and the rEP₄ receptor are different compared to hEP₄, however the poses align nearly identically. Figure 7c features an overlay of the two structures displaying consistent binding poses despite which model was used. The rEP₄ receptor makes polar contacts with PGE₂ via residues Y188^(5.42), S288^(6.48), N324^(7.45), and D65^(2.50) (Fig. 7). The backbone interaction between the 15-hydroxyl-PGE₂/rG103^(3.41) is less significant than the 15-hydroxyl-PGE₂/hS103^(3.41) sidechain interaction. During MD simulation, the 11-hydroxyl of PGE₂ relaxes and interacts with A321 backbone of rEP₄ (Fig. 8). D65^(2.50) loses its direct interaction with

the 11-hydroxyl of PGE₂ after 2 ns (Fig. 8). S288^(6.48), N324^(7.45), I172, Y188^(5.42) make key interactions with PGE₂ through entirety of simulation.

A set of known EP₄ agonists were tested in radioligand binding and cAMP functional activation experiments. The scores from the docking experiment were compared with the functional data to better understand the model predictions (Table 2). Endogenous EP₄ agonists are largely equivalent in both affinity and functional activation within the series with respect to their K_i and EC₅₀ values for either the rEP₄ or hEP₄ receptor, suggesting little species-specific differences in the series. Between the receptors, ligands such as PGE₁, 11-deoxy-PGE₂, and PGE₂ displayed a 0.2–0.3 kcal/mol difference with minimal preference for the human receptor (Table 2).

Within the hEP₄ model, the top scored pose of each agonist was structurally aligned and displayed in Fig. 9. D65^(2.50) H-bonding with γ -lactam hydroxyl is observed in most poses with N321^(7.45) H-bonding with the 15-hydroxyl. Overall, poses are consistent with the hEP₄ model of PGE₂ docking (Fig. 7). The shape of the predicted hEP₄ binding site generated by Site-Map matches well with the poses [30, 31]. The CCL17464,2 pose compared to PGE₂ overlays closely (Fig. 6), despite the different scaffolds. The model's predictions appear to align better with the functional activation data where PGE₁ and PGE₂ trend towards better potency compared to their 11-deoxy counterparts (Table 2). We observed improved scores for both PGE₂

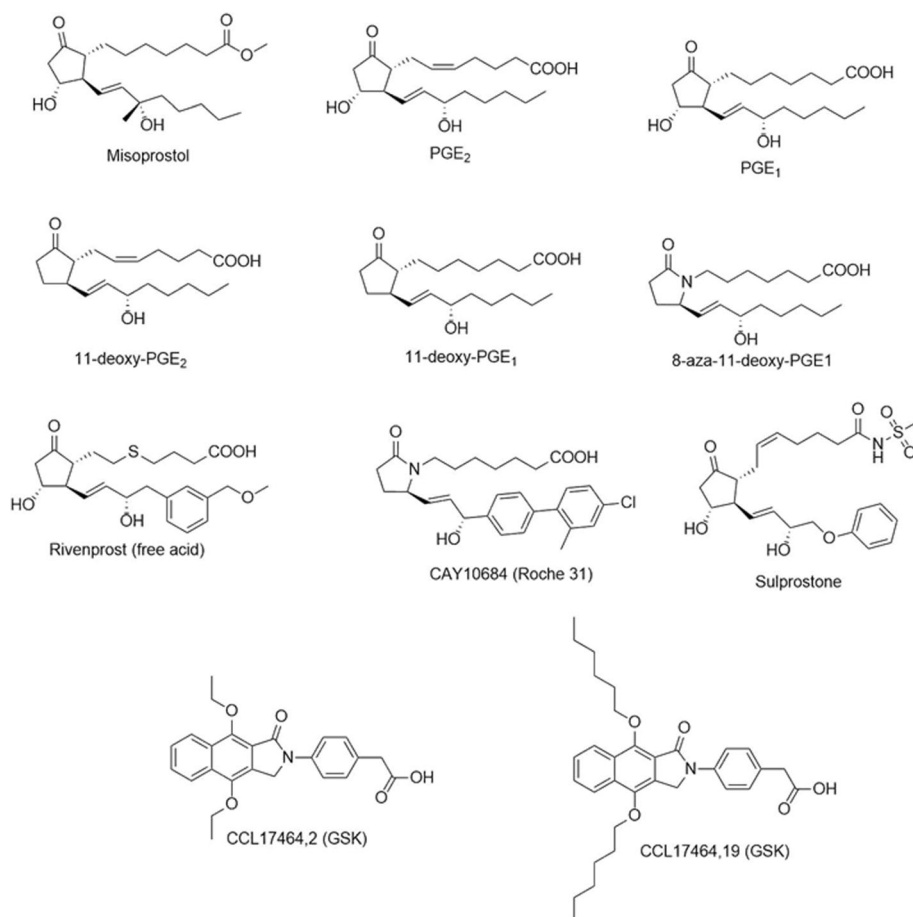


Fig. 4 EP₄ agonists chemical series

and PGE₁ over 11-deoxy-PGE₂ and 11-deoxy-PGE₁ within the model, matching the trend seen with the activation data (Table 2). Likewise, Rivenprost was the top docked compound and is the most potent agonist within the functional activation experiment (Table 2). The model highly favors interaction between D65^(2.50) and the γ -lactam 11-hydroxyl of these agonists. CAY10684 is among the most potent compounds tested in the human cAMP functional activation assay and was among the highest scoring compounds within the human model.

Rivenprost displays a binding mode similar to PGE₂ with D65^(2.50) H-bonding with γ -lactam hydroxyl and N321^(7.45) H-bonding with the 15-hydroxyl. Rivenprost is the only compound which is significantly more potent in the functional activation assay by Unpaired T-test with two-tailed p value ($p < 0.0001$) and is the top scoring compound within this series, additionally supporting the notion that our model correlates well with the functional activation data determined within this study (Table 2). The α -carboxylate of the Rivenprost free acid interacts with S103^(3.41) and S285^(6.48). CAY10684 is observed to be an especially tight binder in the

radioligand binding assay. In the modeled pose, its primary interaction is through a hydrogen-anion interaction between the α -carboxylate and the partially positive hydrogens of S103^(3.41) and S285^(6.48).

Molecular Mechanics/Generalized Born Surface Area ΔG (MM-GBSA) calculations were performed on docked poses of known EP₄ agonists (Table 2). This scoring function ranked Rivenprost and CAY10684 among the highest predicted affinity molecules within the subset of known EP₄ agonists, matching well with the cAMP activation and binding data for these molecules.

Discussion

The homology models of hEP₄ and rEP₄ presented in this study represent an improvement upon the Margan model of hEP₄ [21]. The RaptorX homology model was compared to a Swiss-model structure to directly associate our model versus the same homology modeling techniques used within the Margan study. Overall, our metrics for non-bonded interactions were favored, the global fold was identical, and we observed less significant

Table 2 Direct binding affinities, activation effective concentrations, and docking scores for a series of EP₄ agonists. K_i refers to equilibrium constant for the concentration of agonists to yield displacement of 50% of radiolabeled ligand. $K_i = IC_{50}/(1 \pm [L]/K_d)$. EC_{50} refers to concentration where 50% activation of receptor within cAMP response assay is observed. Docking score is provided in terms of kcal/mol and is an empirical scoring of docked ligand affinity used for rank ordering. Emodel score can be used as a measure of confidence within the model. MMGBSA calculation is a force-field based method to score docked ligand affinity which correlated well with empirical scoring function. Values shown in grey were reported within cited references. N/A refers to data not available within literature. ND refers to data that was not determined within this study

Compound	Human EP ₄ Receptor					Rat EP ₄ Receptor				
	K _i (nM)	EC ₅₀ (nM)	kcal/mol	Emodel	mmGBSA dG	K _i (nM)	EC ₅₀ (nM)	kcal/mol	Emodel	mmGBSA dG
PGE ₂	0.24	0.58 ± 0.07 (30)	-10.6	-90.9	-57.22	0.19	0.48 ± 0.09 (5)	-10.3	-87.4	-62.91
PGE ₁	0.13	0.42 ± 0.72 (6)	-11.2	-85.7	-70.65	0.20	0.50 ± 0.07 (9)	-11.0	-92.2	-68.30
11-deoxy-PGE ₂	0.23	0.66 ± 0.11 (3)	-9.4	-70.7	-48.32	0.42	1.32 ± 0.24 (3)	-9.2	-67.9	-54.80
11-deoxy-PGE ₁	0.13	0.79 ± 0.19 (3)	-9.7	-75.4	-56.17	0.21	1.13 ± 0.15 (3)	-8.5	-69.0	-53.92
CAY10684	0.061	0.18 ± 0.10 (3)	-11.3	-102.5	-60.72	0.057	0.16 ± 0.06 (4)	-10.1	-111.3	-71.32
Rivenprost (free Acid)	0.37	0.14 ± 0.01 (3)	-12.0	-108.0	-81.44	0.35	1.16 ± 0.29 (3)	-14.2	-125.4	-75.68
8-aza-11-deoxy-PGE ₁	1.7	1.77 ± 0.32 (3)	-9.6	82.3	-56.11	ND	2.64 ± 0.62 (3)	-7.4	-79.3	-54.81
Sulprostone[18]	3310	N/A	-12.6	-118.8	-84.01	43600	N/A	-8.6	-100.2	-63.35
Misoprostol[18]	4340	N/A	-10.0	-81.0	-86.77	26300	N/A	-10.4	-80.2	-67.12
CCL17464,2[17]	19.9	N/A	-9.5	-89.1	ND	N/A	N/A	ND	ND	ND
CCL17464,19[17]	>6310	N/A	-4.1	-115.6	ND	N/A	N/A	ND	ND	ND

Z-score outliers. The homology models presented within this study were minimized within an implicit membrane system using the OPLS3 force field while the Margan model used the OPLS2005 force field without a membrane calculation. The Margan model is not available on any public archives for the use of other research groups,

whereas our data is available publicly. Margan referenced site-directed mutagenesis experiments, which identified several key residues for PGE₂ binding including T199^(5.53), S278^(6.41), S285^(6.48), and R316^(7.37) [21]. This study's hEP₄ receptor docking experiments

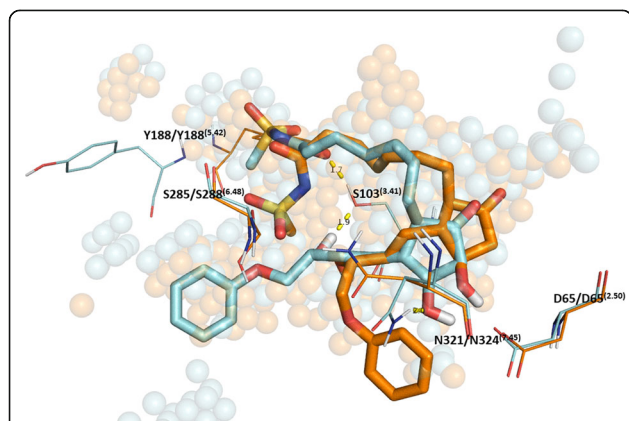


Fig. 5 Docked pose of Sulprostone (orange) in stick representation overlaid within hEP₄ receptor with versus docked pose within rat (teal). Sulprostone scored higher in human receptor and matches the pose of PGE₂ within human receptor but fails to match this pose within rat receptor. Note interactions with S103^(3.41) within human model

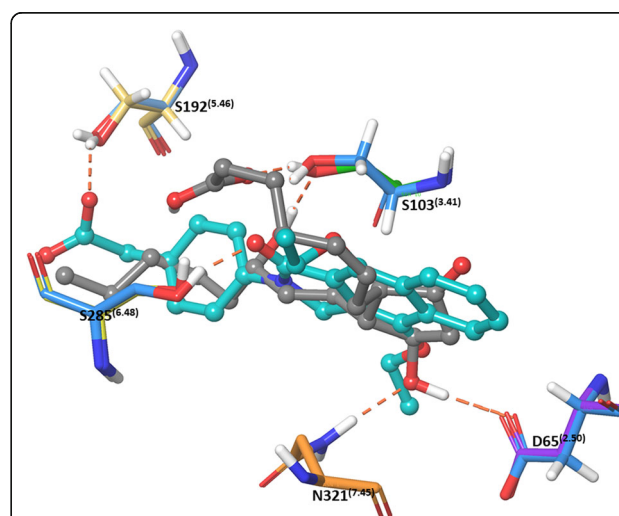
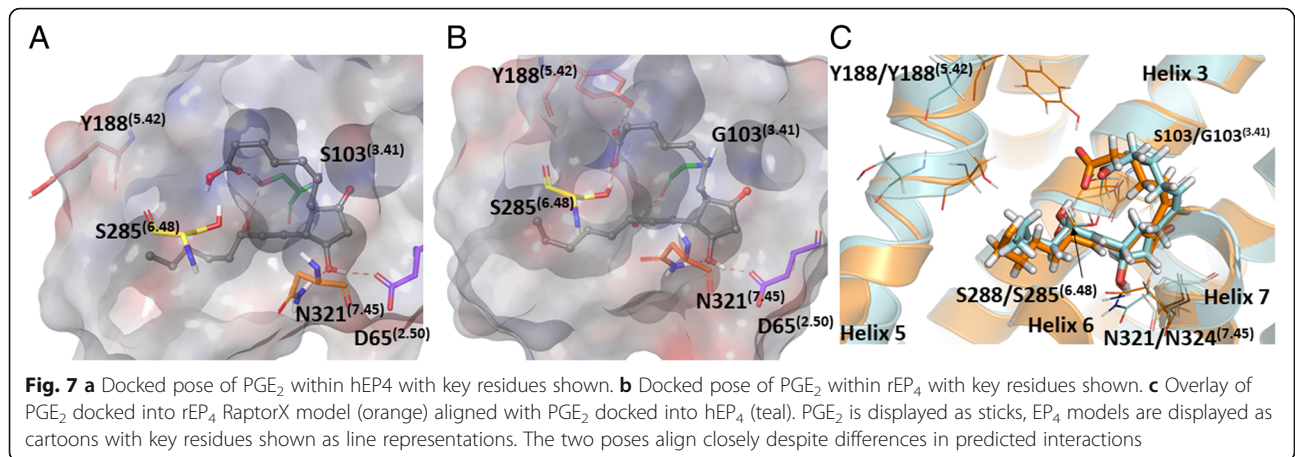


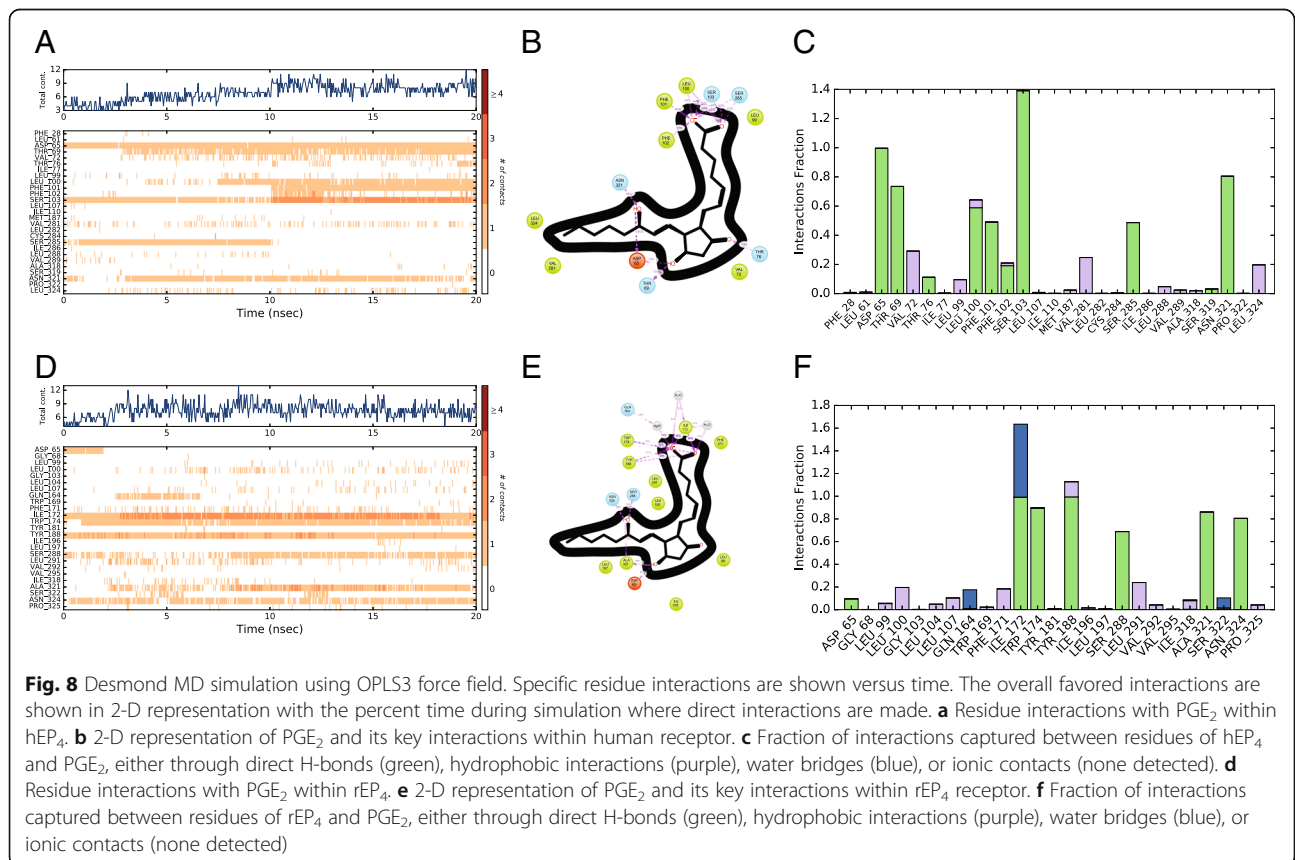
Fig. 6 Docked pose of CCL17464,2 (teal) in stick representation overlaid within human EP₄ receptor with versus docked pose of PGE₂ (grey) within human EP₄ receptor. Key residues are shown as line representations

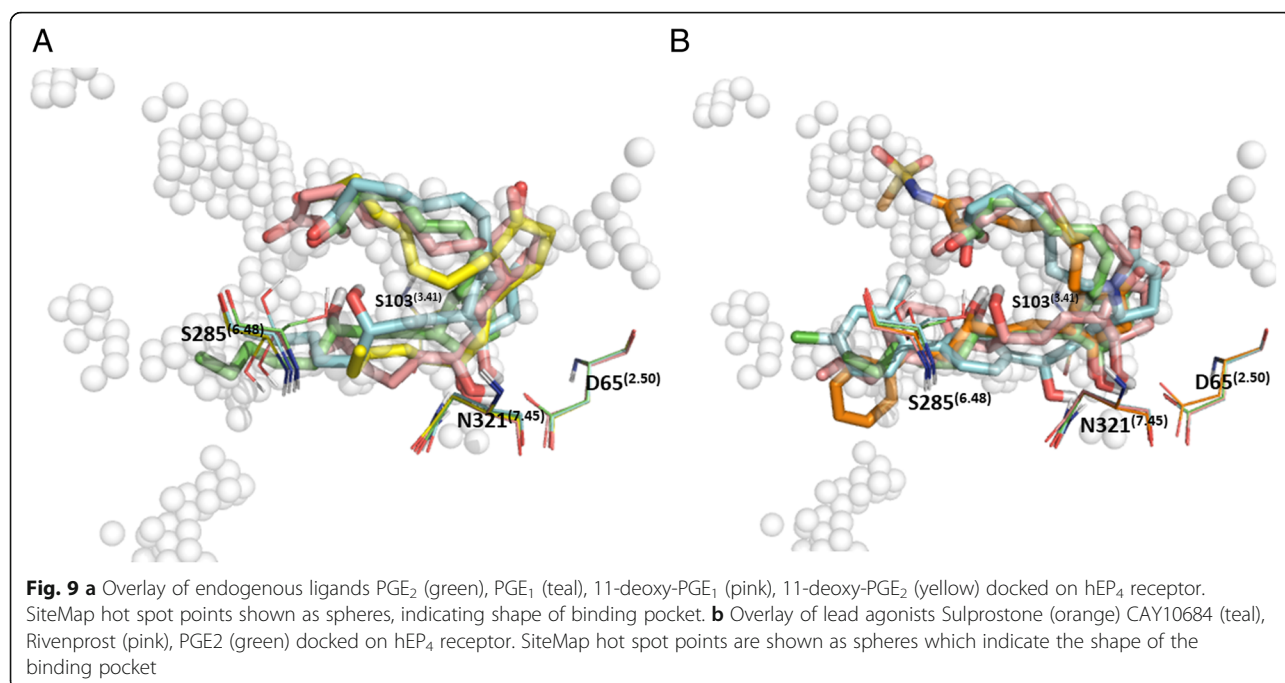


implicate S285^(6.48) through direct H-bond formation to docked PGE₂. T199^(5.53), S278^(6.41) and R316^(7.37) are additionally located within 5 Å of the docked PGE₂ and may play a role within extended H-bonding networks. Together the top pose matches well with the previously reported biological data. Both the Margan study and ours implicate S285^(6.48) and S103^(3.41) as key PGE₂ contacts within hEP₄. Our study implicates several transmembrane helix 2 residues including D65^(2.50) and

T69^{2.54} as polar contacts interacting with 11-hydroxyl of PGE₂.

The poses identified within this study are different than the pose proposed by the Margan model (Additional file 6: Figure S6) [21]. The top poses within this study appear to be deeper within the transmembrane helices region of the receptor. In the Margan model, Y186^(5.40) and F191^(5.45) are shown oriented inwards toward the binding pocket. With the improved solvation of our model, relaxed within





an implicit membrane system, these residues are pointed towards the lipid facing inner membrane region and do not play a significant role in contacting the docked molecules. In agreement with the Margan model, we observe both S285^(6.48) and S103^(3.41) playing a key role interacting with the 15-hydroxyl of PGE₂.

Structural comparison of hEP₄ with the homology model of the human DP prostaglandin receptor bound to an antagonist, displays a RMSD of 4.6 Å [32]. Our binding site aligns with the 3–4–5–6 helix binding site and differs in the reported 1–2–7 antagonist binding site [32]. Our agonists dock closely to the CSxP motif of helix 6, where S285^(6.48) sidechain is 1.8 Å from the α -carboxylate of PGE₂. This motif aligns with the CWxP motif within rhodopsin and other class A GPCRs, where it has been implicated as activation transmission switch [33, 34]. During review of this manuscript, a set of two crystal structures of the Human prostaglandin D2 receptor CRTH2 were released within the Protein Data Bank, although no publication has been yet to be published. These were crystallized with two antagonists bound, fevipiprant (PDB ID: 6D26) and CAY10471 (PDB ID: 6D27). These antagonists bind within the canonical 1–2–7 antagonist binding site, near T168. Structural alignment of the C(S/W) xP motif, shows that the predicted hEP₄ S285^(6.48) is well oriented overlaying with W of the CWxP motif. Likewise, D65^(2.50) overlays well between the models. S103^(3.41) of the hEP₄ structure is closely positioned to either a S118 or M115 residue of DP2 receptor (Additional file 7: Figure S7). Lastly, the crystal structures of human

prostaglandin D2 receptor show Y188^(5.42) and Y186^(5.40) structurally aligning with hydrophobic residues (A205, F211, F215) largely oriented toward the hydrophobic inner-membrane space, and not towards the active site as seen within the Margan model [21].

Previous work identified T168 within the second extracellular loop of hEP₄ as being essential for PGE₂ binding [20]. This residue is observed at the turn of the anti-parallel β -sheets which serve as the cap of the receptor within this model. This is located within the identified antagonist binding site, as seen in DP2 receptor, and likely plays a key role in receptor conformation. T168 is observed making a hydrogen bond with Y80^(2.65), which may be essential for orienting the beta-turn-beta and control of TM helix 2 orientation.

Experimental radioligand competition data and functional activation data was collected within this study providing additional datasets that align with the homology models. The [³H]-PGE₂ binding results are consistent with binding data reported previously such as PGE₂ being measured at a K_i of 0.72 nM against hEP₄ previously and measured as 0.58 nM within this study [19, 35]. The models appear to align better with the rank order of the cAMP activation data versus the competitive binding data. This result may be a consequence of the use of an empirical scoring function for rank ordering. MM-GBSA scores were also determined (Table 2). This is a force-field based method to estimate the free energy of binding by estimating the energy of the complex versus the free receptor and ligand. The rank-order from MM-GBSA did not always align with the empirical scoring, implying this

result may be an artifact of the compounds selected in conjunction with the inherent error in the model's predictions. Lastly, the statistical power behind the radioligand competition experiments was insufficient to determine the significance of those values. Thus, differences between certain compounds may be insignificant.

The model performed much better at predicting the species-specific differences within Sulprostone compared to Misoprostol, when using empirical scoring. This may partly be due to the limited structural differences between Misoprostol and the endogenous EP₄ agonists, where the model fails to capture the significance of 15-methyl in terms of affinity differences. However, using MM-GBSA calculation, the predicted binding difference between the receptors is more significant and the species selectivity is more obvious. Surprisingly, being agonists with μM affinities and primary selectivity for EP₁ & EP₃, the compounds unexpectedly scored well by both empirical scoring and force-field. As the direct binding results for Misoprostol and Sulprostone are presented from the literature, it is unclear if differences within methodologies play a role in this discrepancy. Likewise, this observation points to the inherent limitations to the use of a homology model which likely fails to capture receptor subtype differences that exist between hEP₄, hEP₃, hEP₂, and hEP₁. Of the compounds tested, Rivenprost appears to display the most species-specific selectivity within activation of the EP₄ receptor. For receptor activation, the EC₅₀ was measured to be 0.142 nM and 1.16 nM for hEP₄ and rEP₄, respectively (Table 2). The radioligand experiments estimated the K_s to be 0.37 nM and 0.35 nM for hEP₄ and rEP₄, respectively. MM-GBSA predicts a 5.76 kcal/mol difference in binding to the receptors, suggesting it may support that there is species-selectivity. The model predicts a species difference for CAY10684 with a 10.6 kcal/mol difference, an effect not observed within the *in vitro* functional activation or direct binding studies.

These models provide a resource to enable *in silico* drug discovery and allow for the design of mutational studies to further understand the binding of PGE₂ and EP₄ activation. Mutational studies should be performed to validate these models and their predictions, including G103S in rEP₄, to test if this ablates species-selectivity. The mutations D65A, N324A, S288A, Y188F would be useful for confirming the essential nature of these predicted interactions within rEP₄. Likewise, the mutations D65A, S103G, S103A, S285A, N321A would be informative for confirming the essential nature of these predicted interactions within hEP₄. This model can also be used by researchers for *in silico* alanine scanning to assist in their predictions of binding interactions between these receptors with novel scaffolds. In the absence of an available crystal structure, these models

will allow for hypothesis generation for researchers within the field of prostaglandin biology. Work is on-going to enhance these models including utilizing the data from the prostaglandin D2 receptor to refine these models.

Conclusions

This work has generated a set of novel homology models of the rEP₄ and hEP₄ receptors. The models provide an improvement upon the previously reported structure, largely due to improved solvation by use of an implicit membrane model. Structural statistics and biological data compared to this model support their validity and highlight their limitations. The hEP₄ empirical scoring model appeared to align best with the cAMP activation data in rank order of agonist potency. This rank ordering matches closely with the rEP₄ receptor. The model also successfully rank-ordered two compounds from a previously reported SAR series where the steric bulk of a para substituted di-*p-n*-hexoxy on a non-prostanoid heterocyclic core was disfavored over the di-*p*-ethoxy [18]. Likewise, species-specific differences between these models were highlighted and a test series of known agonists with reported species-selectivity were screened against each model. In both cases, the weak agonists Sulprostone and Misoprostol were known to bind with higher affinity to the human structure [19]. The models generated scores that were substantially higher for the human receptor versus rat for Sulprostone and Misoprostol. The radioligand competition and function activation data presented within this study are similar to the previously reported data. Our agonists dock closely to the CSxP motif of helix 6, where S285^(6.48) sidechain is 1.8 Å from the α -carboxylate of PGE₂. This motif aligns with the CWxP motif within rhodopsin and other class A GPCRs, where it has been implicated as activation transmission switch [33, 34]. These structures are a significant advancement compared to the Margan model and enable *in silico* drug discovery efforts targeting the EP₄ receptor.

Addendum

The work presented within this study using the native and unbiased form of hEP₄, was performed completely independently from the crystal structures of hEP₃ (PDB IDs: 6M9T & 6AK3) and hEP₄ (PDB IDs: 5YHL & 5YWY) [36–39]. Both crystal structures were released on December 5th, 2018, while this manuscript was still in review following our initial submission on June 15th, 2018. Our revised manuscript following reviewers' edits was resubmitted on November 25th, 2018. This addendum was added March 29th, 2019 following final revisions to highlight some features of the crystallographic data.

While the first crystal structure of hEP₄ represents a major milestone for understanding the biology of prostaglandins, the use of homology modeling for this target is still necessary. The published hEP₄ crystal structure used an altered form of the receptor (via thermostable mutations) which stabilized the receptor in its inactive conformation [36]. These mutations and the addition of a bound Fab molecule weighted the receptor toward the inactive form and thus enhancing antagonist binding [36]. Previously, the adenosine receptor A2a had been shown to have a Na⁺ binding pocket with proposed importance to receptor activation [40]. The thermostable mutation G106R^{3,39} presented within the hEP₄ crystal structure likely disrupted this pocket again forcing the structure into an inactive form [36]. As a result, the need for improved models of the active conformation of hEP₄ remains.

The active conformation of the hEP₃ PGE₂-bound structure shows the ω -chain of PGE₂ oriented toward W295^(6,48) of the CWxP motif making a direct interaction with D99^(2,50) of the reported Na⁺ binding pocket [38]. Within the homology model presented in this work, direct interactions to the corresponding S285^(6,48) of the CSxP motif and D65^(2,50) are predicted. As the Na⁺ pocket may serve as a negative regulator, *Morimoto et al 2018* suggested this may be the mechanism for receptor activation [38, 40].

Several residues that make significant interactions with the ONO-AE3-208 ligand in hEP₄ are also highlighted by our docking predictions including L99^(3,31), T76^(2,61), V72^{2,61}, W169^(ECL2) which largely form a hydrophobic pocket near the E ring of PGE₂ [36]. Our model failed to identify Y80/Y114^(2,65), a key contact for the alpha-chain carboxylate observed in both the hEP₃ and hEP₄ crystal structures as a “key” ligand contact. This manuscript, however, did note the potential importance of this residue independently: “T168 is observed making a hydrogen bond with Y80^(2,65), which may be essential for orienting the beta-turn-beta and control of TM helix 2 orientation” (Discussion Section). Additionally, our model also predicts the importance of S103^(3,41), a prediction which requires additional biochemical or structural information to confirm. Similarly, our model highlights the importance of residues within the putative Na⁺ binding pocket including S285^(6,48) and D65^(2,50). We have added a (Additional file 8: Figure S8) showing the induced fit docking of PGE₂ within a homology model based on the hEP₄ crystal structure [36]. Interactions between Y80^(2,65) and R316^(7,40) with the alpha chain carboxylate were observed. The PGE₂ 11-hydroxyl makes hydrogen bond with hEP₄ S69^(2,54) side chain. The carbonyl oxygen appears to also contact T76^(2,61). The PGE₂ 15-hydroxyl is near D65^(2,50) (4.3 Å) and is close to creating D65^(2,50) backbone interactions. In

summary, both corroborating and contradictory data presented in this manuscript, supports many of the contacts highlighted in both the hEP₃ and hEP₄ crystal structures and continues to solidify both the PGE₂-D65 interaction and putative Na⁺ binding pocket which plays a key role in agonist binding and ultimately receptor activation.

Methods

Receptor homology modeling

The sequences for *R. norvegicus* EP₄ (rEP₄) receptor and *H. sapiens* EP₄ (hEP₄) receptor obtained from National Center for Biotechnology Information (NCBI) using accession codes NP_114465.3 and NP_000949.1, respectively. These were submitted to RaptorX structure prediction suite (<http://RaptorX.uchicago.edu/>) and analyzed to confirm the quality of the model using the *P*-value, global distance test, absolute global quality, and RMSD [23, 41–46]. RaptorX utilized squid and human rhodopsin as the primary templates for both rat and human EP₄ threading. A full list of templates is provided in the supplemental. Sequences were additionally submitted to Swiss-model through the Expasy molecular biology suite (<https://swissmodel.expasy.org>) to provide additional models for global comparison. Models were prepared for docking using the protein preparation wizard within Schrödinger Maestro 11, adding hydrogens, creating disulfide bonds, and generating protonation states using Epik at pH 7.0 ± 2.0 [47]. H-bond assignments and torsion angles were optimized using PROPKA and a restrained minimization was performed using OPLS3 force field [48–51]. Loop refinement was performed in the presence of an implicit membrane. Membrane width was estimated by submitting to OPM Membrane Server (<http://opm.phar.umich.edu/server.php>) with values of 30.6 Å for rat EP₄ receptor and 27.5 Å for human EP₄ receptor [52]. Orientation of implicit membrane was completed using the global structure excluding loop residues (1–18, 295–309, 364–402) within the atom specification language (ASL).

Induced fit docking with Schrödinger maestro

All ligand files were prepared and generated within Maestro 11. Ligands were prepared with LIGPREP from SMILES using OPLS3 force field modified using EPIK [22, 49–51, 53, 54]. Molecules were desalted and featured all possible tautomers. Binding site detection was performed using SiteMap with 20 site points required per reported site, using a fine grid, and using a more restrictive definition of hydrophobicity [30, 31]. Initial rigid body docking of PGE₂ was used to center the box for a more extensive Induced Fit docking experiment [47, 55–58]. The glide grid was centered on residues previously identified as being near the binding site including

S103^(3.41), S285^(6.48), S319 and G103^(3.41), S288^(6.48) for human and rat receptors, respectively. Extra precision (XP) protocol was used in Glide with Van der Waals scaling factor set to 1.0 and a partial charge cutoff of 0.15. Following Glide docking, the receptor and top scoring pose were merged and the ligand was selected to center the grid box for induced fit docking [58]. A search grid of 8,000 Å³ was centered on the docked PGE₂. Residues within 5 Å of glide poses were refined using Prime with additional residues being refined as well including S103^(3.41), Y165, I172, Y184^(5.38), Y186^(5.40), F191^(5.45), L195^(5.49), S285^(6.48), D311^(7.35), S319^(7.43) and G103^(3.41), L107^(3.45), W175, Y181, Y188^(5.42), S185^(5.39), S193^(5.47), S288^(6.48) for the human and rat receptors, respectively. Prime refinement incorporated the implicit membrane prepared earlier. Glide redocking was performed within 30 kcal/mol of best structure and for top 20 structures overall using XP protocol. PGE₂ poses were evaluated based on docking score, Emodel score, and GlideScore. Follow-up compounds were docked with the grid centered on the docked pose of PGE₂ using the same settings as above.

Molecular dynamics simulations

Molecular dynamics simulations were prepared with Desmond using the classical simulation system set-up [59]. TIP3P solvent model was implemented and the membrane was placed excluding disordered loops (residues 1–18, 295–309, 364–402) from ASL. The box volume was minimized automatically using an orthorhombic shape. Ions within 20 Å of agonist were excluded and the model was neutralized by the addition of Cl⁻ ions from 0.15 M sodium chloride and solvated using an OLPS3 force field [22, 50, 51]. Simulations were performed for 20 ns with 500 frames. Temperature and pressure were 300 K and 1.01325 bar, respectively. Simulations were analyzed using Schrödinger Maestro Simulation Event Analysis wizard.

EP₄ receptor binding

Radioligand binding experiments were carried out versus the hEP₄ and rEP₄ receptors. Human EP₄ receptor binding was originally determined by Eurofins Pharma Discovery Services (Bois-l'Évêque, France) and confirmed in our laboratory. We also implemented the rEP₄ receptor binding studies. Equilibrium competition binding assays were conducted to determine the inhibition constants (K_i) for ligand interactions with EP₄ receptors sourced from membranes (160,000×g) of HEK293 cells overexpressing recombinant hEP₄ or rEP₄ receptors. Ligand competitions were conducted from 30 nM to 30 pM against [H³]-PGE₂ (180 Ci/mmol; NEN Radiochemicals, Boston, MA), which was held constant at 0.5 nM. Assays were performed in 10 mM 2-(N-morpholino) ethanesulphonic acid (MES) buffer

containing 1 mM EDTA and 10 mM MnCl₂, pH 6.0, during 120 min at room temperature. K_i was calculated using the Cheng Prusoff equation where $K_i = IC_{50}/(1 \pm L/K_d)$. A Scatchard plot was used to determine K_d for [H³]-PGE₂. The calculated K_d for [H³]-PGE₂ was 0.3 nM.

EP₄ receptor functional activation

Human and rat EP₄ receptors were expressed in HEK293T/17 cells separately by reverse transfection on 96-well plates with optimized amounts of cDNA expression constructs immobilized on the surface. Activation of EP₄ receptor in this cell line was measured as an increase in cAMP levels using an ELISA kit (Cayman Chemical, Ann Arbor MI). In short, the transfection plates were seeded with 50,000–80,000 cells/well in reduced serum medium containing 0.5% FBS and incubated overnight at 37 °C with 5% CO₂. Before stimulation with test compounds, media was aspirated from the wells and replaced with reduced serum media containing 0.5 mM 3-isobutyl 1-methylxanthine (IBMX). Compound dilution series were prepared in the same IBMX containing media at 2X final concentration and applied to the wells in equal volume. Stimulation media were aspirated from the plates after 30 min incubation with test compounds, and the plates with cells were placed on dry ice and then put into –80 °C freezer for >2 h. Cell lysates were prepared on thawed plates by adding 200 µl/well ice-cold ELISA buffer with 0.05% Tween-20 followed by titration. The cell lysates were then transferred to a polypropylene plate and clarified by centrifugation at 1000×g for 15 min at 4 °C. Supernatant was transferred into a pre-coated mouse Anti-Rabbit IgG ELISA plate together with serial dilutions of cAMP for a standard curve in triplicate. cAMP-acetylcholinesterase conjugate (cAMP tracer) was added, followed by cAMP EIA antiserum. Plates were incubated overnight with shaking. After washing 5 times in washing buffer, Ellman's reagent was added to the well and shake for 90 min under cover before measuring absorbance at 405 nm on a plate reader.

Additional files

Additional file 1 : Figure S1. (A) Swiss-model Ramachandran plots for the hEP₄ model. (B) RaptorX Ramachandran plots for the hEP₄ model. (C) RaptorX Ramachandran plots for the rEP₄ model. Plots were similar for hEP₄ and rEP₄ for the residues within favored regions (90.25%/88.09% of residues, human/rat) and allowed regions (5.75%/6.70%, human/rat). Swiss-model displayed improved Ramachandran plot versus RaptorX. (PNG 173 kb)

Additional file 2 : Figure S2. (A) Z-score outliers for hEP₄ RaptorX model (B) Z-score outliers for hEP₄ Swiss-model. Red lines indicate residues with Z-score warnings. Green corresponds to near ideal Z-scores. (PNG 133 kb)

Additional file 3 : Figure S3. MD simulation Ligand RMSD v. Time (20 ns) for (A) hEP₄ and (B) rEP₄. (PNG 91 kb)

Additional file 4 : Figure S4. MD simulation Protein RMSF v. residue (during 20 ns simulation) for (A) hEP₄ and (B) rEP₄. Smoothed curve over 5 neighboring residues to reduce noise. Red areas indicate alpha helical regions. Green lines indicate ligand contacts. Brown line indicates RMSF for sidechains. Blue line indicates Ca RMSF. Red line indicates B factor, shown only on hEP₄ plot. (PNG 132 kb)

Additional file 5 : Figure S5. Representative image of Emodel scores versus Docking score for a set of agonists docked into hEP₄. (PNG 77 kb)

Additional file 6 : Figure S6. Side by side comparison of the hEP₄ docked PGE₂ poses between the Margan model [20] and this study from the same angle. (PNG 525 kb)

Additional file 7 : Figure S7. Alignment of PGE₂ docked to hEP₄ with Crystal structure of the prostaglandin D2 receptor CRTH2 with fevipreant. Top down view of receptor with transmembrane helices numbered. hEP₄ receptor is display in rainbow coloring. DP2 receptor is shown in teal. Key residues for predicted hEP₄ agonist binding site are shown with the corresponding DP2 residues overlaid. C(S/W) xP motif overlays between models with W of the CWxP motif overlaying with S285^(6,48). D65^(2,50) overlays well between the models. S103^(3,41) of the hEP₄ structure is closely positioned to either a S118 or M115 residue of DP2 receptor. (PNG 1136 kb)

Additional file 8 : Figure S8. Homology model of the hEP₄ receptor docked with PGE₂. All 5 poses output from an induced fit protocol are shown [45, 53–56]. PGE₂ is displayed in ball and stick representation with non-polar hydrogens hidden (gray). Dotted lines indicate hydrogen bonding interactions. hEP₄-PGE₂ interactions include: (1) The alpha chain carboxylate to both Y80^(2,65), and R316^(7,40) (2) The 11-hydroxyl to the OH group of S69^(2,54) (3) The carbonyl oxygen/T76^(2,61) and (4) The 15-hydroxyl to D65^(2,50) is 4.3 Å and within proximity to the hEP₄ backbone. NOTE: This figure is part of the addendum and added to the original manuscript on March 29th, 2019. All other sections of this report were prepared prior to December 5th, 2018 release of EP₄ crystal structure. (PNG 451 kb)

Additional file 9 : Table S1. RaptorX threading model statistics, before minimized refinement within Maestro. (DOCX 14 kb)

Abbreviations

COX: Cyclooxygenase; hEP₄: human prostaglandin E2 receptor subtype 4; MM-GBSA: Molecular Mechanics-Generalized Born Surface Area; PGE₁: Prostaglandin E1; PGE₂: prostaglandin E2; rEP₄: rat prostaglandin E2 receptor subtype 4

Acknowledgements

The authors would like to thank Carrie Johnson for her collection of functional activation data within rEP₄ receptor. The authors would like to thank Rana Sidhu for his contributions to collection of hEP₄ radioligand binding data.

Authors' contributions

MCH generated the homology models, performed MD simulations, performed docking experiments, and prepared manuscript. AJS and MCH designed the general scope of the project. AJS oversaw execution of in silico work. CSH collected human EP₄ cAMP activation data and lead development of this assay. MIM collected rEP₄ direct binding data and requisitioned hEP₄ direct binding data. MIM and SDB provided biological and chemical context for this study and suggested which compounds to use as control compounds. All authors read and approved the final manuscript.

Authors' information

M.C.H. is a Scientist within the Medicinal Chemistry Group at Cayman Chemical Co. C.S.H is Manager of Cell Biology at Cayman Chemical Co. M.I.M. is Director of Drug Discovery at Cayman Chemical Co. S.D.B. is VP of Chemistry at Cayman Chemical Co. A.J.S. is VP of Biochemistry at Cayman Chemical Co.

Funding

All funds for this study were R&D expenditures of Cayman Chemical Co.

Availability of data and materials

All models reported here have been deposited within the ModelArchive (<https://www.modelarchive.org/>). hEP₄ (DOI: <https://doi.org/10.5452/ma-aasgt>) & rEP₄ (DOI: <https://doi.org/10.5452/ma-aio8z>).

Ethics approval and consent to participate

No human participants, data, or tissues were used within this study.

Consent for publication

Not applicable.

Competing interests

The authors declare that they have no competing interests.

Received: 17 May 2019 Accepted: 11 July 2019

Published online: 27 August 2019

References

- Sugimoto Y, Narumiya S. Prostaglandin E receptors. *J Biol Chem*. 2007; 282(16):11613–7.
- Markovic T, Jakopin Z, Dolenc MS, Mlinaric-Rascan I. Structural features of subtype-selective EP receptor modulators. *Drug Discov Today*. 2017; 22(1):57–71.
- Blackwell KA, Raisz LG, Pilbeam CC. Prostaglandins in bone: bad cop, good cop? *Trends Endocrinol Metab*. 2010;21(5):294–301.
- Jiang GL, Nieves A, Im WB, Old DW, Dinh DT, Wheeler L. The prevention of colitis by E Prostanoid receptor 4 agonist through enhancement of epithelium survival and regeneration. *J Pharmacol Exp Ther*. 2007;320(1):22–8.
- Konya V, Marsche G, Schuligoi R, Heinemann A. E-type prostanoid receptor 4 (EP4) in disease and therapy. *Pharmacol Ther*. 2013;138(3):485–502.
- Araki Y, Suganami A, Endo S, Masuda Y, Fukushima K, Regan JW, Murayama T, Tamura Y, Fujino H. PGE1 and E3 show lower efficacies than E2 to beta-catenin-mediated activity as biased ligands of EP4 prostanoid receptors. *FEBS Lett*. 2017;591(22):3771–80.
- Yokoyama U, Iwatsubo K, Umemura M, Fujita T, Ishikawa Y. The prostanoid EP4 receptor and its signaling pathway. *Pharmacol Rev*. 2013;65(3):1010–52.
- Barrett SD, Holt MC, Kramer JB, Germain B, Ho CS, Ciske FL, Kornilov A, Colombo JM, Uzieblo A, O'Malley JP et al: Difluoromethylene at the gamma-Lactam alpha-Position Improves 11-Deoxy-8-aza-PGE1 Series EP4 Receptor Binding and Activity: 11-Deoxy-10,10-difluoro-8-aza-PGE1 Analog (KMN-159) as a Potent EP4 Agonist. *J Med Chem*. 2019, 62(9):4731–4741.
- Kambe T, Maruyama T, Nakai Y, Oida H, Maruyama T, Abe N, Nishiura A, Nakai H, Toda M. Synthesis and evaluation of gamma-lactam analogs of PGE (2) as EP4 and EP2/EP4 agonists. *Bioorg Med Chem*. 2012;20(11):3502–22.
- Ke HZ, Crawford DT, Qi H, Simmons HA, Owen TA, Paralkar VM, Li M, Lu B, Grasser WA, Cameron KO, et al. A nonprostanoid EP4 receptor selective prostaglandin E2 agonist restores bone mass and strength in aged, ovariectomized rats. *J Bone Miner Res*. 2006;21(4):565–75.
- El-Nefrawy N, Abdel-Hakim K, Kanayama N. The selective prostaglandin EP4 agonist, APS-999 Na, induces follicular growth and maturation in the rat ovary. *Eur J Endocrinol*. 2005;152(2):315–23.
- Vukicevic S, Simic P, Borovecki F, Grgurevic L, Rogic D, Orlic I, Grasser WA, Thompson DD, Paralkar VM. Role of EP2 and EP4 receptor-selective agonists of prostaglandin E (2) in acute and chronic kidney failure. *Kidney Int*. 2006; 70(6):1099–106.
- Hishikari K, Suzuki J, Ogawa M, Isobe K, Takahashi T, Onishi M, Takayama K, Isobe M. Pharmacological activation of the prostaglandin E2 receptor EP4 improves cardiac function after myocardial ischaemia/reperfusion injury. *Cardiovasc Res*. 2009;81(1):123–32.
- Yoshida K, Oida H, Kobayashi T, Maruyama T, Tanaka M, Katayama T, Yamaguchi K, Segi E, Tsuboyama T, Matsushita M, et al. Stimulation of bone formation and prevention of bone loss by prostaglandin E EP4 receptor activation. *Proc Natl Acad Sci U S A*. 2002;99(7):4580–5.
- Marui A, Hirose K, Maruyama T, Arai Y, Huang Y, Doi K, Ikeda T, Komeda M. Prostaglandin E2 EP4 receptor-selective agonist facilitates sternal healing after harvesting bilateral internal thoracic arteries in diabetic rats. *J Thorac Cardiovasc Surg*. 2006;131(3):587–93.
- Elworthy TR, Kertesz DJ, Kim W, Roepel MG, Quattrocchio-Setti L, Smith DB, Tracy JL, Chow A, Li F, Brill ER, et al. Lactams as EP4 prostanoid receptor

- subtype selective agonists. Part 1: 2-Pyrrolidinones-stereochemical and lower side-chain optimization. *Bioorg Med Chem Lett*. 2004;14(7):1655–9.
17. Spisani S, Vicenzi E, Traniello S, Pollini GP, Barco A. Synthetic prostaglandin analogue: in vitro studies on human neutrophils. *Immunopharmacology*. 1982;4(4):323–30.
 18. Healy MP, Allan AC, Bailey K, Billinton A, Chessell IP, Clayton NM, Giblin GMP, Kay MA, Khaznadar T, Michel AD, et al. Discovery of {4-[4,9-bis(ethoxy)-1-oxo-1,3-dihydro-2H-benzo [f]isoindol-2-yl]-2-fluorophenyl} acetic acid (GSK726701A), a novel EP₄ receptor partial agonist for the treatment of pain. *Bioorg Med Chem Lett*. 2018;28(10):1892–6.
 19. Davis TL, Sharif NA. Pharmacological characterization of the [³H]-prostaglandin E₂ binding to the cloned human EP₄ prostanoid receptor. *Br J Pharmacol*. 2000;130:1919–26.
 20. Brett A, Stillman LA, Breyer RM. A conserved threonine in the second extracellular loop of the human EP₂ and EP₃ receptors is required for ligand binding. *Eur J Pharmacol*. 1998;357:73–82.
 21. Daniela Margan AB, Mracec M, Mracec M. 3D homology model of the human prostaglandin E₂ Receptor EP₄ subtype. *Rev Roum Chim*. 2012; 57(1):39–44.
 22. Harder E, Damm W, Maple J, Wu C, Reboul M, Xiang JY, Wang L, Lupyán D, Dahlgren MK, Knight JL, et al. OPLS3: a force field providing broad coverage of drug-like small molecules and proteins. *J Chem Theory Comput*. 2016;12(1):281–96.
 23. Kallberg M, Wang H, Wang S, Peng J, Wang Z, Lu H, Xu J. Template-based protein structure modeling using the RaptorX web server. *Nat Protoc*. 2012;7(8):1511–22.
 24. Haas J, Roth S, Arnold K, Kiefer F, Schmidt T, Bordoli L, Schwede T. The Protein Model Portal—a comprehensive resource for protein structure and model information. *Database (Oxford)*. 2013;2013:bat031.
 25. Schwede T, Sali A, Honig B, Levitt M, Berman HM, Jones D, Brenner SE, Burley SK, Das R, Dokholyan NV, et al. Outcome of a workshop on applications of protein models in biomedical research. *Structure (London, England : 1993)*. 2009;17(2):151–9.
 26. Di Tommaso P, Moretti S, Xenarios I, Orobitg M, Montanyola A, Chang J-M, Taly J-F, Notredame C. T-Coffee: a web server for the multiple sequence alignment of protein and RNA sequences using structural information and homology extension. *Nucleic Acids Res*. 2011;39(Web Server issue):W13–7.
 27. Notredame C, Higgins DG, Heringa J. T-coffee: a novel method for fast and accurate multiple sequence alignment. *J Mol Biol*. 2000;302(1):205–17.
 28. Colovos C, Yeates TO. Verification of protein structures: patterns of nonbonded atomic interactions. *Protein Sci*. 1993;2:1511–9.
 29. Shimamura T, Hiraki K, Takahashi N, Hori T, Ago H, Masuda K, Takio K, Ishiguro M, Miyano M. Crystal Structure of Squid Rhodopsin with Intracellularly Extended Cytoplasmic Region. *J Bio Chem*. 2008;283(26): 17753–17756.
 30. Halgren T. New method for fast and accurate binding-site identification and analysis. *Chem Biol Drug Des*. 2007;69(2):146–8.
 31. Halgren TA. Identifying and characterizing binding sites and assessing Druggability. *J Chem Inf Model*. 2009;49(2):377–89.
 32. Shankar V, Goddard WA 3rd, Kim SK, Abrol R, Liu F. The 3D structure of human DP prostaglandin G-protein-coupled receptor bound to Cyclopentanoidole antagonist, predicted using the DuplexBiHelix modification of the GENSeMBLE method. *J Chem Theory Comput*. 2018; 14(3):1624–42.
 33. Venkatakrishnan AJ, Deupi X, Lebon G, Tate CG, Schertler GF, Babu MM. Molecular signatures of G-protein-coupled receptors. *Nature*. 2013;494:185.
 34. Olivella M, Caltabiano G, Cordero A. The role of Cysteine 6.47 in class A GPCRs. *BMC Struct Biol*. 2013;13(1):3.
 35. Boie Y, Stocco R, Sawyer N, Slipetz DM, Ungrin MD, Neuschafer-Rube F, Puschel GP, Metters KM, Abramovitz M. Molecular cloning and characterization of the four rat prostaglandin E₂ prostanoid receptor subtypes. *Eur J Pharmacol*. 1997;340:227–41.
 36. Toyoda Y, Morimoto K, Suno R, Horita S, Yamashita K, Hirata K, Sekiguchi Y, Yasuda S, Shiroishi M, Shimizu T, et al. Ligand binding to human prostaglandin E receptor EP₄ at the lipid-bilayer interface. *Nat Chem Biol*. 2019;15(1):18–26.
 37. Audet M, White KL, Breton B, Zarzycka B, Han GW, Lu Y, Gati C, Batyuk A, Popov P, Velasquez J, et al. Crystal structure of misoprostol bound to the labor inducer prostaglandin E₂ receptor. *Nat Chem Biol*. 2019;15(1):11–7.
 38. Morimoto K, Suno R, Hotta Y, Yamashita K, Hirata K, Yamamoto M, Narumiya S, Iwata S, Kobayashi T. Crystal structure of the endogenous agonist-bound prostanoid receptor EP₃. *Nat Chem Biol*. 2019;15(1):8–10.
 39. Hollenstein K. Structures shed light on prostanoid signaling. *Nat Chem Biol*. 2019;15(1):3–5.
 40. Fan H, Chen S, Yuan X, Han S, Zhang H, Xia W, Xu Y, Zhao Q, Wu B. Structural basis for ligand recognition of the human thromboxane A₂ receptor. *Nat Chem Biol*. 2019;15(1):27–33.
 41. Ma J, Peng J, Wang S, Xu J. A conditional neural fields model for protein threading. *Bioinformatics*. 2012;28(12):i59–66.
 42. Ma J, Wang S, Zhao F, Xu J. Protein threading using context-specific alignment potential. *Bioinformatics*. 2013;29(13):257–65.
 43. Peng J, Xu J. Low-homology protein threading. *Bioinformatics*. 2010; 26(12):i294–300.
 44. Peng J, Xu J. Boosting protein threading accuracy. *Res Comput Mol Biol*. 2009;5541:31–45.
 45. Peng J, Xu J. A multiple-template approach to protein threading. *Proteins*. 2011;79(6):1930–9.
 46. Peng J, Xu J. RaptorX: exploiting structure information for protein alignment by statistical inference. *Proteins*. 2011;79(Suppl 10):161–71.
 47. Madhavi Sastry G, Adzhigirey M, Day T, Annabhimoju R, Sherman W. Protein and ligand preparation: parameters, protocols, and influence on virtual screening enrichments. *J Comput Aided Mol Des*. 2013;27(3):221–34.
 48. Jorgensen W, Tirado-Rives J. The OPLS [optimized potentials for liquid simulations] Potential Functions for Proteins, Energy Minimization for Crystals of Cyclic Peptides and Crambin. *J Am Chem Soc*. 1988; 110(6): 1657–66.
 49. Jacobson MP, Pincus DL, Rapp CS, Day T, Honig B, Shaw DE, Friesner RA. A hierarchical approach to all-atom protein loop prediction. *Proteins*. 2004; 55(2):351–67.
 50. Jorgensen WL, Maxwell DS, Tirado-Rives J. Development and testing of the OPLS all-atom force field on conformational energetics and properties of organic liquids. *J Am Chem Soc*. 1996;118(45):11225–36.
 51. Shivakumar D, Williams J, Wu Y, Damm W, Shelley J, Sherman W. Prediction of absolute solvation free energies using molecular dynamics free energy perturbation and the OPLS force field. *J Chem Theory Comput*. 2010;6(5):1509–19.
 52. Lomize MA, Pogozheva ID, Joo H, Mosberg HI, Lomize AL. OPM database and PPM web server: resources for positioning of proteins in membranes. *Nucleic Acids Res*. 2012;40(Database issue):D370–6.
 53. Greenwood JR, Calkins D, Sullivan AP, Shelley JC. Towards the comprehensive, rapid, and accurate prediction of the favorable tautomeric states of drug-like molecules in aqueous solution. *J Comput Aided Mol Des*. 2010;24(6):591–604.
 54. Shelley JC, Cholleti A, Frye LL, Greenwood JR, Timlin MR, Uchimaya M. Epik: a software program for pK_a prediction and protonation state generation for drug-like molecules. *J Comput Aided Mol Des*. 2007;21(12):681–91.
 55. Friesner RA, Banks JL, Murphy RB, Halgren TA, Klicic JJ, Mainz DT, Repasky MP, Knoll EH, Shelley M, Perry JK, et al. Glide: a new approach for rapid, accurate docking and scoring. 1. Method and assessment of docking accuracy. *J Med Chem*. 2004;47(7):1739–49.
 56. Friesner RA, Murphy RB, Repasky MP, Frye LL, Greenwood JR, Halgren TA, Sanschagrin PC, Mainz DT. Extra precision glide: docking and scoring incorporating a model of hydrophobic enclosure for protein–ligand complexes. *J Med Chem*. 2006;49(21):6177–96.
 57. Halgren TA, Murphy RB, Friesner RA, Beard HS, Frye LL, Pollard WT, Banks JL. Glide: a new approach for rapid, accurate docking and scoring. 2. Enrichment factors in database screening. *J Med Chem*. 2004;47(7):1750–9.
 58. Sherman W, Beard HS, Farid R. Use of an induced fit receptor structure in virtual screening. *Chem Biol Drug Des*. 2006;67(1):83–4.
 59. Bowers KJ, Chow E, Xu H, Dror RO, Eastwood MP, Gregersen BA, Klepeis JL, Kolosvary I, Moraes MA, Sacerdoti FD, Salmon JK, Shan Y, Shaw DE. Scalable Algorithms for Molecular Dynamics Simulations on Commodity Clusters. Proceedings of the ACM/IEEE Conference on Supercomputing (SC06). In: Tampa: ACM; 2006.

Publisher's Note

Springer Nature remains neutral with regard to jurisdictional claims in published maps and institutional affiliations.